

# Photonic Quantum Computing

Jacquiline Romero and Gerard Milburn

Australian Research Council Centre of Excellence for Engineered Quantum Systems and  
School of Mathematics and Physics, University of Queensland, QLD 4072, Australia

## Summary

Photonic quantum computation refers to quantum computation that uses photons as the physical system for doing the quantum computation. Photons are ideal quantum systems because they operate at room temperature, and photonic technologies are relatively mature. The field is largely divided between discrete- and continuous-variable photonic quantum computation. In discrete-variable (DV) photonic quantum computation, quantum information is represented by one or more modal properties (e.g. polarization) that take on distinct values from a finite set. Quantum information is processed via operations on these modal properties (e.g. waveplates in the case of polarization), and eventually measured using single photon detectors. In continuous-variable (CV) photonic quantum computation, quantum information is represented by properties of the electromagnetic field that take on any value in an interval (e.g. position). The electromagnetic field is transformed via Gaussian and non-Gaussian operations, and then detected via homodyne detection. Both CV and DV photonic quantum computation have been realized experimentally and they each have a unique set of challenges that need to be overcome to achieve scalable photonic universal quantum computation. It is possible to combine both DV and CV in a hybrid CV-DV fashion to overcome the limitations of either individual approach.

**Keywords:** qubit, qudit, continuous variable, entanglement, squeezing, measurement, measurement-based quantum computation, universal gates, cluster states, fault tolerance, quantum error correction

## 1 Introduction

Quantum computation is a paradigm of computation that exploits the properties of quantum systems to perform computation. Information embodied in quantum systems follows the rules of quantum mechanics. Using quantum computation, specific computational tasks, e.g. finding the prime factors of a composite number, can be performed more efficiently. The potential for such an advantage has fuelled both theory and practical implementations of quantum computation.

The theory of quantum computations is agnostic to the physical system—a quantum bit (qubit) is represented by the same vector regardless of the physical system that implements the quantum computation. The physical system can be based on matter, e.g. trapped ions and superconducting qubits, or based on photons, referred to as photonic quantum computation.

While the 2020s has been characterised by the noisy intermediate-scale quantum (NISQ) computers that are mostly based on matter systems, photonic systems remain a strong contender for a future large-scale universal quantum computer for many reasons. (1) Characteristic quantum phenomena like quantum superposition, interference, and entanglement can be observed and engineered in photons at

room temperature, in contrast to the low temperature that is often needed for quantum systems based on matter. (2) A photon interacts very weakly with its environment thereby maintaining the coherence that is required throughout the quantum computation. (3) A photon is a rich system that is amenable to engineering using relatively mature technologies. For example, while the gate operations on matter systems ultimately depend on natural properties like interaction strength between a qubit and an external field, gate operations on a photonic quantum computer depend on classical parameters that can be engineered. (4) Photons can be entangled over long distances. If we are to have a network of quantum computers in the future, making the photon as the carrier of quantum information makes sense for connectivity and modularity.

This article will focus on the development of photonic quantum computing, from early proposals of linear optical quantum computation to the leading photonic quantum computing architecture to date.

## 2 DiVincenzo criteria for quantum computation

In 2000, Di Vincenzo listed a set of criteria that is required for the realisation of quantum computation (DiVincenzo [2000]). These criteria are rooted in the circuit model of quantum computation but not limited to the circuit model. The following paragraphs list these criteria and evaluate how a photonic quantum system fares against them:

**Well-defined state space of qubits.** A photon has different properties that can be used as a qubit. The presence or absence of a photon in a particular mode (e.g. horizontal polarization) can be taken as the qubit. This is called single-rail encoding. Since a photon can be described by multiple modes, it is also possible to use the presence or absence of a photon (i.e. the number) in either of two orthogonal modes as a qubit. Taking horizontal and vertical polarizations as the orthogonal modes, the qubit state can be written (in the number basis) as  $c_0 |10\rangle + c_1 |01\rangle$ . This is called dual-rail encoding. Taking the most general definition of a mode, as an eigenfunction of a Hermitian operator that describes a linear physical system (Miller [2019]), it is apparent that the number of modes is not limited to two. It is possible to have other types of encodings that make use of more modes (e.g.  $d$ -rail encoding using  $d$  number of spatial modes). Photonic technology is relatively mature. The state space defined by the various optical modes are experimentally accessible with high accuracy, hence photonic qubits can be well-characterized. Taking polarization as example, an off-the-shelf polarizing beamsplitter distinguishes between the horizontal and vertical polarizations with an error in the order of  $10^{-5}$ .

**Ability to initialise the state of the qubits.** The system of qubits that will be used for computation should be initialised to a known quantum state, just in the same way that a classical register is initialised to a known state. This initialisation could be as simple as a product state of  $n$  qubits,  $|0\rangle \otimes |0\rangle \otimes \dots \otimes |0\rangle$  which can then be manipulated by quantum gates to lead to a desired quantum state. The requirement for initialisation is also important for quantum error correction (QEC). The QEC in a quantum computer is expected to use up a lot of qubits (Brun [2020]; Devitt et al. [2013]), hence the requirement for a continuous supply of new qubits that are in a known initial state. It is best that the time to initialise the qubits (initialisation time) is relatively shorter than the gate operation times. Using photons presents the advantage that there is no inherently natural limit to the initialisation time, in contrast to matter systems which has an associated cooling or relaxation time. Photons can be initialised to  $|0\rangle$  easily enough by putting them all in the same mode. The challenge lies in creating the multi-photon state, because these usually depend on non-deterministic processes such as spontaneous parametric down-conversion (SPDC) or spontaneous four-wave mixing (SFWM). The initialisation time for photons largely depends on engineering. Nevertheless, recent developments in deterministic single photon generation and photonic quantum gates inspire some optimism.

**Long relevant decoherence times.** A quantum system in contact with an environment will eventually decohere. In the most extreme case, the decoherence time may be taken as the time it takes for a superposition,  $c_0 |0\rangle + c_1 |1\rangle$ , to become a mixture,  $c_0 |0\rangle\langle 0| + c_1 |1\rangle\langle 1|$ . The decoherence time should be much longer than the gate operation times, and how much longer will depend strongly on the QEC being used. The decoherence time for a photon is very long because a photon interacts very weakly with its environment. However, there are other factors (e.g. dispersion, dephasing, and loss) that affect the complex amplitudes of a superposition. These factors are detrimental to quantum computation, but can be minimized by error mitigation and QEC techniques. How a quantum state changes depends very much on the physical system itself—decoherence is highly system-specific—and careful characterization is required. Such characterization is arguably easier for photons because a photon, aside from not interacting with the environment, also does not interact with other photons. Hence, the correlation of decoherence between neighbouring qubits is not an issue unlike in matter-based quantum systems.

**A universal set of quantum gates.** Quantum computation is typically a sequence of unitary transformations acting on one or more qubits. A set of quantum gates is universal if composing gates belonging to the set enables one to approximate any unitary transformation with arbitrary accuracy. The specification of universal gate sets is agnostic to the physical system used for quantum computation but the implementations are highly dependent on the physical systems. Photons present the advantage that arbitrary single-qubit operations can be expressed as combinations of beamsplitters and phase-shifters—an optical interferometer. The time to do a sequence of single-qubit operations is short, it is simply the time it takes for the photon to traverse the interferometer. This is in contrast to matter-based systems that use pulses for single-qubit operations, where an adiabatic approximation is required (Plenio and Knight, PRA 1996), and where the operation time is determined by the time interval such that the overlap between successive pulses is negligible. The implementation of two-qubit gates is a challenge for photons. The fact that photons do not interact also means that it is difficult for the operation on one photon depend on the state of the other. Using the optical Kerr nonlinearity is a way to do photonic two-qubit gates, but this is weak and lossy. The most promising approach so far is based on linear optics (KLM, Fusion, this will be discussed in detail in Sec. 6). The success rate is not 100%, but the success of the two-qubit gate is heralded.

**A qubit-specific measurement capability.** The result of the computation can be obtained from the final state of the quantum system. The final state needs to be measured in order to obtain the classical information, e.g. “0” with probability  $p$ , and “1” with probability  $1-p$ . Efficient projective measurements are therefore necessary for quantum computation. Projective measurements of photonic quantum states are relatively well-developed for a variety of photonic properties. The efficiency is a function of the losses in the photonic system and minimizing loss is central to photonic quantum computing efforts.

### 3 Photonic quantum information: discrete vs continuous

A photon is a rich physical system that can be associated with various physical properties. Some of these physical properties are *discrete variables* in that they can take on only distinct values (e.g. polarisation), while some are *continuous variables* (e.g. electric field) and can take on any value in an interval. Discrete variable quantum computation (DVQC) uses discrete variables embodied in discrete properties, while continuous variable quantum computation (CVQC) uses continuous variables embodied in continuous properties.

In DVQC, a quantum state is written as a superposition of orthogonal vectors  $\{|j\rangle\}$  that correspond to distinct eigenstates,

$$|\psi\rangle = \sum_j c_j |j\rangle \quad (1)$$

where  $j$  is an integer that serves as a label for the vectors in the finite set  $\{|j\rangle\}$  and  $c_j$  are complex coefficients. The coefficients  $c_j$  are normalised,  $\sum_i |c_j|^2 = 1$ . Polarisation is a qubit i.e., the number of vectors in the set ( $\{|j\rangle\}$ ) is two. The superposition of these two vectors can be used to describe all possible (pure) polarisation states. Other photonic properties accommodate a qudit description, i.e.  $\{|j\rangle\} = d$ . For example, any (pure) transverse spatial profile can be expressed as a superposition of functions  $\{u_j\}$  that are solutions to the wave equation. Although the number of these functions is theoretically infinite, the physical system (e.g. the physical aperture) imposes a limit on  $d$ . In a similar way to dual-rail encoding, one can have  $d$ -rail encoding with the state of the qudit written as  $c_0 |100\dots\rangle + c_1 |010\dots\rangle + c_d |000\dots 1\rangle$ .

In CVQC (Gottesman et al. [2001]), a quantum state is written as a superposition over eigenstates of operators with a continuous rather than discrete spectrum, for example position  $\hat{q}$  and momentum,  $\hat{p}$ , of a free particle. These are canonically conjugate operators, so that  $[\hat{q}, \hat{p}] = i$ . In this article we are using units such that  $\hbar = 1$ . This means that action, and angular momentum, are in units of  $\hbar$ . In Dirac notation we write,

$$\hat{q} = \int_{-\infty}^{\infty} dq q |q\rangle \langle q|, \quad \hat{p} = \int_{-\infty}^{\infty} dp p |p\rangle \langle p| \quad (2)$$

where  $\langle q'|q\rangle = \delta(q' - q)$ ,  $\langle p'|p\rangle = \delta(p' - p)$ . The canonical commutation relations require that  $\langle q|p\rangle = \frac{1}{\sqrt{2\pi}} e^{-iqp}$ . Given an arbitrary state  $|\psi\rangle$  we can write

$$|\psi\rangle = \int_{-\infty}^{+\infty} dq \psi(q) |q\rangle = \int_{-\infty}^{+\infty} dp \tilde{\psi}(p) |p\rangle \quad (3)$$

where

$$\tilde{\psi}(p) = \frac{1}{2\pi} \int_{-\infty}^{\infty} dq e^{-ipq} \psi(q) \quad (4)$$

are Fourier transform pairs. Here,  $q, p$  are real variables and  $\psi(q), \tilde{\psi}(p)$  are complex-valued, continuous function of  $q, p$  respectively. Note that while we sometimes write the ket  $|q\rangle$  as if it was a state, it is not a physical state. It has delta-function normalisation and does not lie in the Hilbert space of square integrable functions. This is just a statement of the Heisenberg uncertainty principle: there are no physical states that have zero uncertainty in position or momentum, or more physically, such states cannot be prepared by a finite sequence of physical operations, although we can get arbitrarily close given sufficient resources.

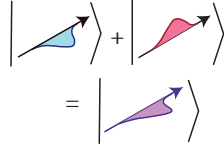
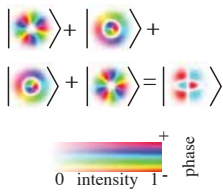
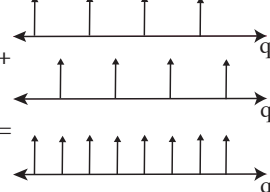
Table 1 shows the correspondence for qubits, qudits, and CV, together with some physical examples using photons.

## 4 Optical modes

What is the Hilbert space of a photon? A photon is a single particle excitation of an optical field *mode*. There is potential for confusion here. We like to think of a photon as a single 'particle' in the sense of non-relativistic quantum mechanics, but in quantum field theory the Hilbert space is associated with orthonormal modes of the electromagnetic (EM) field. A single photon state can then be a single excitation of a single mode or a superposition of a single photon state of many modes for example  $|1\rangle = \sum_k f_k a_k^\dagger |0\rangle$  (where  $f_k$  are complex coefficients and  $a_k^\dagger$  is a creation operator that will be defined shortly). The Hilbert is associated with the mode itself. The Hilbert space of each mode is mathematically equivalent to the Hilbert space of a simple harmonic oscillator. The total Hilbert space of the EM field is the tensor product Hilbert space of many modes.

For each orthonormal mode indexed by  $k$  we define annihilation and creation operators  $a_k, a_k^\dagger$  where  $[a_k, a_{k'}^\dagger] = \delta_{kk'}$ . The electric field can then be written as (Walls and Milburn [2008]),

Table 1: Discrete and continuous photonic quantum information

|                  | Qubit   | Qudit   | Continuous Variable (CV)   |
|------------------|---|---|--|
| basis vectors    | $\{ 0\rangle,  1\rangle\}$  | $\{ 0\rangle,  1\rangle, \dots,  d\rangle\}$  | $\{ q\rangle\} \in \mathbb{R}$   |
| orthogonality    | $\langle \ell   m \rangle = \delta_{\ell, m}$<br>$\ell, m \in \{0, 1\}$                           | $\langle \ell   m \rangle = \delta_{\ell, m}$<br>$\ell, m \in \{0, 1, \dots, d\}$                             | $\langle q_1   q_2 \rangle = \delta(q_1 - q_2)$<br>$q_1, q_2 \in \mathbb{R}$                     |
| quantum state    | $ \psi\rangle = c_0 0\rangle + c_1 1\rangle$  | $ \psi\rangle = c_0 0\rangle + c_1 1\rangle + \dots + c_d d\rangle$   | $ \psi\rangle = \int_{-\infty}^{+\infty} dq \psi(q)  q\rangle$                                   |
| physical example | polarisation<br> | transverse spatial modes<br> | quadrature<br> |

$$\mathbf{E}(\mathbf{r}, t) = i \sum_k \left( \frac{\hbar \omega_k}{2\epsilon_0} \right)^{1/2} \left[ a_k \mathbf{u}_k(\mathbf{r}) e^{-i\omega_k t} - a_k^\dagger \mathbf{u}_k^*(\mathbf{r}) e^{i\omega_k t} \right] \quad (5)$$

where  $\omega_k = c|\vec{k}|$  and  $\{\mathbf{u}_k(\mathbf{r})\}$  are spatial mode functions that satisfy

$$\begin{aligned} \left( \nabla^2 + \frac{\omega_k}{c^2} \right) \mathbf{u}_k(\mathbf{r}) &= 0 \\ \int_V \mathbf{u}_k^*(\mathbf{r}) \mathbf{u}_l(\mathbf{r}) d\mathbf{r} &= \delta_{kl}. \end{aligned} \quad (6)$$

The operator with a discrete spectrum is the number operator for mode  $k$ ,  $a_k^\dagger a_k$

$$a_k^\dagger a_k |n\rangle_k = n |n\rangle_k \quad n = 0, 1, 2, \dots \quad (7)$$

The operators with a continuous spectrum for mode  $k$  are

$$q_k = \frac{1}{\sqrt{2}} (a_k + a_k^\dagger), \quad p_k = -i \frac{1}{\sqrt{2}} (a_k - a_k^\dagger) \quad (8)$$

where  $[q_k, p_{k'}] = i\delta_{kk'}$ . It then follows that we can use the continuous representation previously discussed.

## 5 Optical qubits

### 5.1 Number state qubit encoding

Let  $k$  be a generic index for a field mode with wave vector  $\vec{k}$  and polarisation vector  $\vec{\epsilon}$ . We can encode a qubit as a single photon excitation of two orthonormal field modes

$$|0\rangle = a_{k_1}^\dagger |0\rangle = |1\rangle_{k_1} \otimes |0\rangle_{k_2}, \quad (9)$$

$$|1\rangle = a_{k_2}^\dagger |0\rangle = |0\rangle_{k_1} \otimes |1\rangle_{k_2}. \quad (10)$$

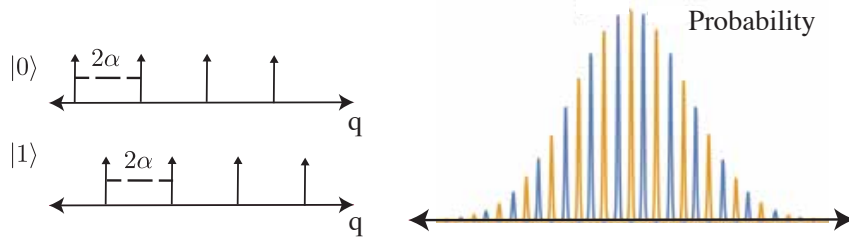


Figure 1: GKP encoding. Ideal infinitely squeezed states separated by  $2\alpha$  (left) are encoded as a coherent superposition of Gaussian modes (right).

where  $|0\rangle$  is the vacuum state of the total field. This is called *dual-rail encoding*. This decoding is simply done by a photon number resolving measurement of each mode, i.e. one that can clearly distinguish  $|n\rangle_k$  from  $|n \pm 1\rangle_k$ . An arbitrary qubit state is then a single excitation eigenstate of total photon number  $\hat{N} = \sum_k a_k^\dagger a_k$ ,

$$|\psi\rangle = \cos\theta |1\rangle_{k_1} \otimes |0\rangle_{k_2} + \sin\theta e^{-i\phi} |0\rangle_{k_1} \otimes |1\rangle_{k_2}. \quad (11)$$

where  $\theta, \phi$  parameterise a point on the unit sphere in spherical polar coordinates, there are uncountable many qubit states.

## 5.2 Continuous variable qubit encoding

The first CV encoding scheme in the context of encoding a qubit in the states of a harmonic oscillator, was proposed by Gottesmann, Kitaev and Preskill (Gottesman et al. [2001]). It is known as the GKP encoding. As each optical field mode is equivalent to a quantised harmonic oscillator, this scheme can be used for CV encoding of optical qubits. A different encoding based on coherent oscillator states was proposed by Ralph et al. (Ralph et al. [2003]). We begin with the GKP states.

In terms of the continuous spectrum of the quadrature phase operator  $q$  defined in Eq. (8), we encode the logical qubits as (Gottesman et al. [2001])

$$\begin{aligned} |\tilde{0}\rangle &= N_0 \sum_{s=-\infty}^{\infty} e^{-\frac{1}{2}\kappa^2(2s\alpha)^2} T(2s\alpha) |\psi_0\rangle, \\ |\tilde{1}\rangle &= N_1 \sum_{s=-\infty}^{\infty} e^{-\frac{1}{2}\kappa^2[(2s+1)\alpha]^2} T[(2s+1)\alpha] |\psi_0\rangle, \end{aligned} \quad (12)$$

where  $N_{0,1}$  are normalization factors,  $T(a)$  translates  $q$  by  $a$ ,  $\alpha$  is a real number, and  $\kappa^{-1}$  is the width of the Gaussian envelope that weighs the sum of the Gaussians in Eq. 12. The encoding should ideally consist of infinitely squeezed states in both  $q$  and  $p$ , but this is not physically possible. Instead, the ideal encoding is approximated by a coherent superposition of Gaussian modes as in Eq. 12 (hence the notation  $|\tilde{0}\rangle$  and  $|\tilde{1}\rangle$ , Figure 1). The GKP encoding is of great interest because it is an example of a shift-resistant code. Using GKP encoding for an  $n$ -dimensional system, errors resulting from Pauli operators  $\bar{Z} = e^{2\pi i q/n\alpha}$  and  $\bar{X} = e^{-ip\alpha}$ , which cause a shift of  $2\pi/n\alpha$  (for  $p$ ) and  $\alpha$  (for  $q$ ) respectively, can be protected against shifts  $\Delta q$  and  $\Delta p$ :

$$\begin{aligned} |\Delta q| &< \frac{\alpha}{2}, \\ |\Delta p| &< \frac{\pi}{n\alpha}. \end{aligned} \quad (13)$$

Konno et al (Konno [2023]) gave the first experimental demonstration of GKP states in a travelling wave optical system using conditional homodyne measurements and feed-forward. The required nonlinearity in their scheme is introduced off-line by conditional generation of cat states using photon number measurements. In fact, cat states can be used to directly encode optical qubits (Ralph et al. [2003]).

A laser outputs a coherent state  $|\alpha\rangle$ , where  $\alpha$  is a complex number that determines the average field

amplitude. The coherent state  $|\alpha\rangle$  arises from a unitary transformation of the vacuum state  $|0\rangle$ ,  $|\alpha\rangle = D(\alpha)|0\rangle$ , where  $D(\alpha)$  is a displacement operator. These states are not orthogonal, the overlap is given by  $|\langle\alpha|-\alpha\rangle|^2 = e^{-4\alpha^2}$ , but can be very small (e.g. for  $\alpha \leq 2$  the overlaps is  $\sim 10^{-7}$ ). To make an orthogonal encoding, the parity eigenstates can be used:

$$\begin{aligned} |0\rangle &= \mathcal{N}_+^{-1} (|\alpha\rangle + |-\alpha\rangle) \\ |1\rangle &= \mathcal{N}_-^{-1} (|\alpha\rangle - |-\alpha\rangle). \end{aligned} \quad (14)$$

where  $\mathcal{N}_\pm = 2 \pm 2e^{-2|\alpha|^2}$ . These states are referred to as the even and odd cat states. There have been plenty of experimental demonstrations of the generation of cat (and kitten) states, starting with (Ourjoumtsev et al. [2006]).

## 6 Optical gates

In Section 5 we defined a number state encoding for optical qubits. For this encoding to be useful we need to specify how such states can be generated as well as how to perform arbitrary single qubit unitary transformations. We will discuss generation below. Single qubit transformations are relatively easy. Suppose the two modes used in the encoding are two orthogonal travelling wave modes at the input to an arbitrary beamsplitter. The input ( $a_k$ ) and output ( $\bar{a}_k$ ) modes are related by

$$\bar{a}_1 = \cos\theta a_1 + \sin\theta a_2 \quad (15)$$

$$\bar{a}_2 = \cos\theta a_2 - \sin\theta a_1 \quad (16)$$

where  $\cos^2\theta$  is the transmittivity coefficient for each mode. The minus sign in the second equation follows from time reversal invariance of Maxwell's equations. It implies that the transformation can be given in terms of a unitary transformation  $\bar{a}_j = U_{bs}^\dagger(\theta, \phi) a_j U_{bs}(\theta, \phi)$  with

$$U_{bs}(\theta, \phi) = e^{\theta(a_1^\dagger a_2 - a_1 a_2^\dagger)} \quad (17)$$

We then see that

$$U_{bs}(\theta, \phi)|\mathbf{0}\rangle = \cos\theta|\mathbf{0}\rangle + \sin\theta|\mathbf{1}\rangle \quad (18)$$

$$U_{bs}(\theta, \phi)|\mathbf{1}\rangle = \cos\theta|\mathbf{1}\rangle - \sin\theta|\mathbf{0}\rangle \quad (19)$$

is a single qubit transformation we will refer to as the beamsplitter transformation. We refer to the unitary  $U(\theta, \phi)$  as a single qubit *gate*. The unitary operator

$$U_p(\delta) = e^{-i\delta(a_1^\dagger a_1 - a_2^\dagger a_2)} \quad (20)$$

is another single qubit gate defined by

$$U_p(\delta)|\mathbf{0}\rangle = e^{-i\delta}|\mathbf{0}\rangle \quad (21)$$

$$U_p(\delta)|\mathbf{1}\rangle = e^{i\delta}|\mathbf{1}\rangle \quad (22)$$

This is called the phase gate as it introduces a relative phase of  $2\delta$  between the two modes. A combination of the beam-splitter and relative phase gates generate an arbitrary single qubit state. It is easy to see that both these gates leave the total photon number invariant. We refer to such gates as *linear optical gates*.

In order to produce an arbitrary state in the tensor product Hilbert space of two qubits we need a two mode transformation that entangles two dual-rail qubits. It was discovered many years ago that this would require a nonlinear optical process such as four-wave mixing (Yamamoto et al. [1988]; Milburn [1989a]). Unfortunately such optical nonlinearities are very small at single photon intensities. Two *measurement based* protocols were discovered that overcame this problem.

Knill, Laflamme and Milburn (KLM) (Knill et al. [2001]) discovered that conditional states produced by conditioning on single photon counting is sufficient to entangle photonic qubits when all other gates are linear optical gates (they conserve total photon number). This led to the first proposal for linear optical quantum computing (LOQC). Pitman, Jacobs and Franson (Pittman et al. [2002]) discovered a different approach based on conditional photon counting that exploits the ability for spontaneous parametric down conversion (SPDC) to entangle two optical modes. This does not conserve total photon number but it is well understood and easy to implement. It is also the key idea for fusion gates (Browne and Rudolph [2005]), currently the most practical way to do photonic quantum computing. We will describe the LOQC scheme first.

Linear in LOQC refers to the use of linear optical elements, e.g. beamsplitters and phase gate, which act linearly on the input modes  $\hat{a}_k^\dagger$ . The output of a linear optical element is given by the sum

$$\hat{b}_j^\dagger = \sum_k M_{jk} \hat{a}_k^\dagger \quad (23)$$

where  $M_{jk}$  are elements of a unitary matrix. This does not mix creation and annihilation operators so conserves the total photon number. Because any single-qubit state can be generated by a combination of a beamsplitter and a phase gate, it follows that this combination can also be used for any single-qubit gate.

The KLM protocol introduced a way of implementing two-qubit gates using only single-qubit gates, single-photon sources, and detectors that can resolve 0,1, and 2 photons, together with post-selection, a form of measurement-based control. Post-selection can be used in situations where a gate may not always apply the correct transformation but failure is 'heralded', typically by recording a photon count. We only use the gate in a circuit if success is heralded. This is called post-selection. KLM proposed using post-selection to prepare entangled states as a resource for implementing gates. This is possible using gate-teleportation. Generating heralded entangled states of  $n$  photons in  $2n$  modes can then be used to make gate teleportation near deterministic at the expense of many optical components and many trials. The resource overhead for gate teleportation is high. These techniques can be made fault tolerant for photon loss, detector inefficiency, and phase decoherence.

The starting point is to nondeterministically implement the nonlinear sign shift (NS) gate which transforms  $\alpha_0|0\rangle + \alpha_1|1\rangle + \alpha_2|2\rangle \rightarrow \alpha_0|0\rangle + \alpha_1|1\rangle - \alpha_2|2\rangle$ . The *NS* transformation is nonlinear, but KLM showed that this is possible with just linear optics using two extra modes (the ancilla modes), and photodetection. Dual-rail encoding uses at most one photon per mode for encoding. Implementing the NS gate moves outside of the code space but this is easily done using Hong-Ou-Mandle (HOM) (Hong et al. [1987]) interference. This is a nonclassical optical interference at fourth order in the field amplitude.

In Fig. 2, the top input (mode 1) corresponds to  $|\psi\rangle_1 = \alpha_0|0\rangle_1 + \alpha_1|1\rangle_1 + \alpha_2|2\rangle_1$ , and modes 2 and 3 correspond to the ancilla modes. When the input to the NS gate is  $|\psi\rangle_1 \otimes |1\rangle_2 \otimes |0\rangle_3$ , and the angles in Fig. 2 are set as  $\theta_1 = 22.5^\circ, \phi_1 = 0^\circ, \theta_2 = 65.5302^\circ, \phi_2 = 0^\circ, \theta_3 = -22.5^\circ, \phi_3 = 0^\circ$  and  $\phi_4 = 180^\circ$ , the output in mode 1 is  $NS|\psi\rangle_1 = \alpha_0|0\rangle_1 + \alpha_1|1\rangle_1 - \alpha_2|2\rangle_1$ , as long as the output on mode 2 is  $|1\rangle_2$  and the output on mode 3 is  $|0\rangle_3$ . The success rate with this post-selection is  $1/4$ .

The NS gates are important because two of them make up a make a non deterministic conditional sign flip, or a CZ gate:  $|Q_1\rangle|Q_2\rangle \rightarrow (-1)^{Q_1 Q_2} |Q_1\rangle|Q_2\rangle$ , where  $Q_1$  and  $Q_2$  are dual-rail encoded qubits

Fig. 3. The CZ gate comprising of two NS gates succeeds 1/16 of the time, but the times that the gate fails can be determined easily because those are just the times when the ancilla modes of the NS gate are not  $|10\rangle$ . CZ gates and single-qubit gates can be used to implement CNOT gates, a universal quantum computation gate.

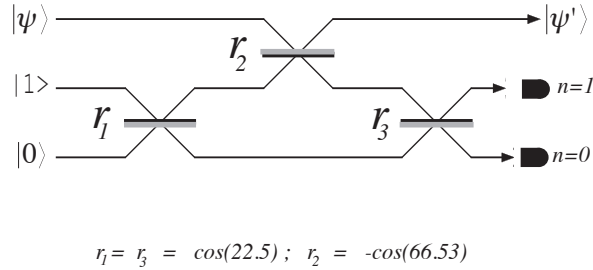


Figure 2: Nonlinear sign shift gate (Knill et al. [2001]). The input to mode 1 (top input) is  $|\psi\rangle_1 = \alpha_0 |0\rangle_1 + \alpha_1 |1\rangle_1 + \alpha_2 |2\rangle_1$ . If a photon is detected in mode 2, and no photon is detected in mode 3, the output of the gate is  $NS|\psi\rangle_1 = \alpha_0 |0\rangle_1 + \alpha_1 |1\rangle_1 - \alpha_2 |2\rangle_1$ . The success probability of the gate is 1/4.

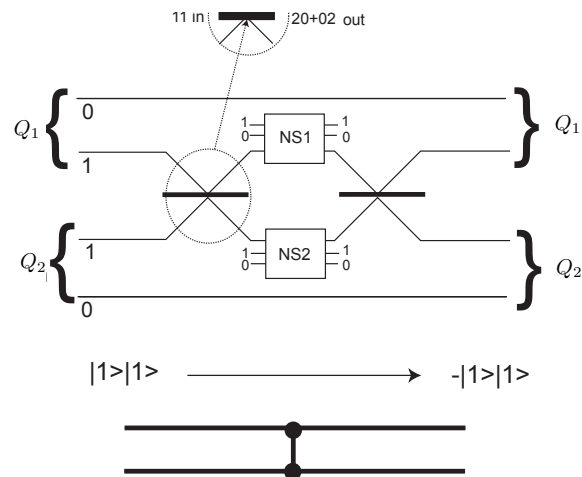


Figure 3: Control-Z (CZ) gate (Knill et al. [2001]). Two NS gates can be used to make a CZ gate by exploiting the HOM effect (insert). The gates acts on  $Q_1$  and  $Q_2$  (dual-rail qubits) as  $|Q_1\rangle|Q_2\rangle \rightarrow (-1)^{Q_1 Q_2} |Q_1\rangle|Q_2\rangle$ . The first beam-splitter ( $45^\circ$ ), leads to the state  $|20\rangle_{13} + |02\rangle_{13}$  when there is 1 photon input to modes 1 and 3. The second beam-splitter undoes this Hong-Ou-Mandel interference after the action of the two NS gates. The success probability is 1/16.

The KLM scheme pointed the way to quantum computing using photon but requires a huge number of optical elements and control electronics: to implement a KLM CZ gate with 95% success probability requires of the order of  $10^{14}$  operations! At about the same time as KLM, Pittman, Jacobs and Franson (Pittman et al. [2002]) made use of a readily available photonic entangling resource — spontaneous parametric down conversion (SPDC) — to implement a different kind of conditional gate. Nielsen(Nielsen [2004]), building on KLM and the concept of measurement based quantum computation (MBQC)(Briegel et al. [2009]), proposed a simpler scheme that avoided gate teleportation. Browne and Rudolph (Browne and Rudolph [2005]), used SPDC sources together with Nielsen’s scheme to give a protocol that dramatically reduced the resources required for optical quantum computing making it a practical technology for quantum computation.

MBQC is implemented on a special class of entangled states called cluster states. First take  $N$  qubits

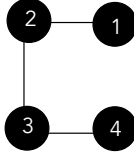


Figure 4: A cluster state example. Each qubit is represented by a node in the graph. A CZ gate is applied between pairs of qubits connected by an edge. Here  $CZ_{12}CZ_{23}CZ_{34}|++++\rangle = \frac{1}{2}(|0+0+\rangle + |0-1-\rangle + |1-0+\rangle + |1+1-\rangle)$

all prepared in the logical  $|0\rangle$  state. Represent each qubit as a node in a two dimensional graph. Apply a H gate to each one  $H : |0\rangle \rightarrow |0\rangle + |1\rangle$  and then apply a CZ gate between all qubits connected by an edge. An example is shown in Fig. 4 for a four-qubit cluster state. Each row of a cluster represents one *logical qubit*. Cluster state computation requires making single qubit measurements on one or more qubits in a cluster and then applying conditional single qubit gate on the remaining qubits, conditional on the outcome of the measurements. For example, given the cluster state

$$|\psi_{\text{in}}\rangle = |i_1\rangle_1 \otimes |+\rangle_2 \otimes |+\rangle_3 \otimes |i_4\rangle_4 . \quad (24)$$

where  $i_1, i_4 \in \{0, 1\}$ . We create a cluster state by applying the CZ gate,

$$S = \exp\left(-i\frac{\pi}{4}\left(\sigma_z^{(1)}\sigma_z^{(2)} + \sigma_z^{(2)}\sigma_z^{(3)} + \sigma_z^{(3)}\sigma_z^{(4)}\right)\right). \quad (25)$$

Note that as this operator commutes with all the  $Z$  Paulis, it does not change the statistics for product Pauli measurements. As the state Eq. (24) has no  $Z$ -correlations, when we measure any qubit in the cluster state is simply disconnected from the cluster, and does not change the remaining links. A  $\sigma_x$  measurement is made on qubit 1 and qubit 2. The measurement outcomes are labelled,  $s_j \in \{0, 1\}$ . The conditional states are

$$|\psi_{\text{out}}\rangle = |s_1\rangle_1 \otimes |s_2\rangle_2 \otimes U_{\text{con}}|i_1 + i_4 \bmod 2\rangle_3 \otimes |i_4\rangle_4, \quad (26)$$

where we apply the conditional single qubit control

$$U_{\text{con}} = \frac{1}{\sqrt{2}}(1 + (-1)^{s_2}i)e^{-i\frac{\pi}{4}(1+\sigma_y^{(3)})}\left(\sigma_x^{(3)}\right)^{s_2} \quad (27)$$

This implements a CNOT of the two input qubit states up to a local control, with the output encoded on the third qubit in the cluster. Given a quantum circuit for logical qubits, we need to determine the sequence of measurement and control to be implemented on the cluster. Another example using the cluster in Fig. 4 is shown in Fig. 5.

The CZ entangling can be done unitarily given a large cross-Kerr nonlinearity(Hutchinson and Milburn [2004]). However, in a photonic dual-rail code, we need to implement this step using a conditional (post-selected) nondeterministic gate. This can be done using the KLM teleportation scheme but there is a better way using fusion gates of Browne and Rudolph(Browne and Rudolph [2005]). The elements of the scheme are:

- code physical qubits as single photons in polarisation modes,  $(H, V)$ .
- use polarisation rotations to measure qubits in arbitrary basis.
- instead of CZ gates between clusters use probabilistic **fusion gates**.
- fusion operators are measurement based operations that take two qubits to one:  $|0\rangle\langle 00| + |1\rangle\langle 11|$

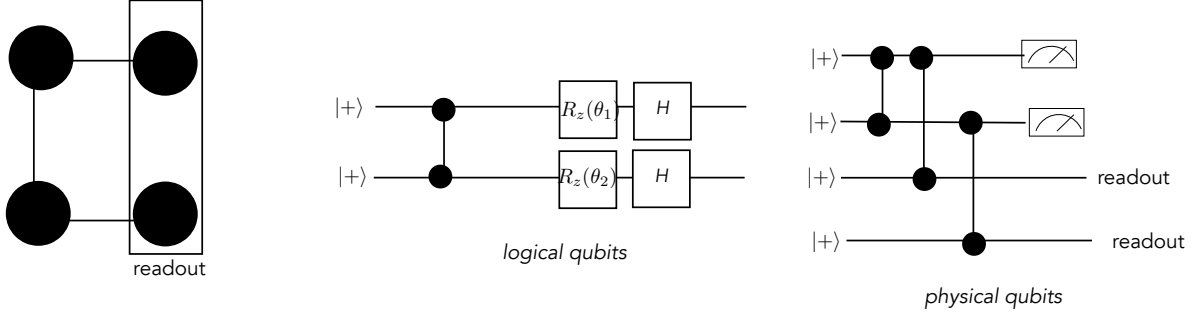


Figure 5: The equivalence between a cluster state for MBQC (left) and a quantum circuit for logical qubits (middle). The last vertex in a cluster row is the readout qubit. On the right we show the creation of the cluster followed by measurements in the computational basis. Depending on the outcome of the measurements, the logical circuit is implemented where the Z-rotation gate parameter depends on the measurement outcomes. For example if the measurement outcome is 00, we get  $\theta_1 = \pi, \theta_2 = 0$ . The single qubit rotation gate is defined by  $R_z(\theta)|+\rangle = |0\rangle + e^{i\theta}|1\rangle$

- replace two qubits with a single qubit while retaining all cluster state bonds on each qubit.

SPDC sources can produce two photons entangled in polarisation. It is then easy to create Bell pairs of the form

$$|0\rangle|+\rangle + |1\rangle|-\rangle \quad (28)$$

where  $|\pm\rangle = |H\rangle \pm |V\rangle$ . In a polarisation dual-rail qubit encoding, this is a two-qubit ‘cluster state’ of the form  $|0\rangle|+\rangle + |1\rangle|-\rangle$ . We refer to it as a Bell-pair cluster.

Using a polarising beam-splitter this two photon state may be separated into two distinct spatial and polarised modes. This enables a Bell pair fusion gate (Fig. 6). As one mode is measured, there is only one transmitted output mode. The state of this mode however is conditioned on the photon count. If

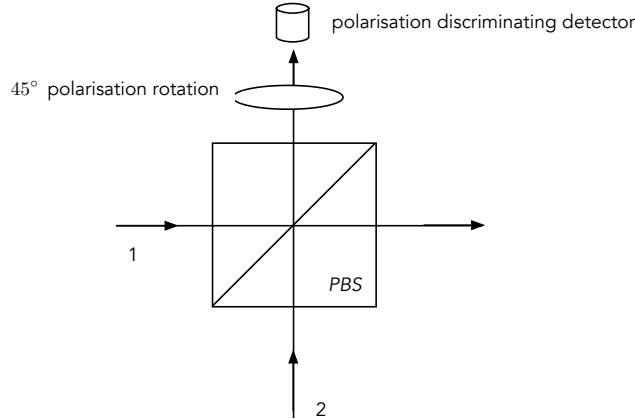


Figure 6: Type-I fusion. On a polarising beamsplitter, all horizontally polarised photons are transmitted while all vertically polarised photons are reflected. This is followed by a linear optical element that rotates the plane of polarisation by  $\pi/4$  and then a single photon detector. This effects a change of measurement basis for a polarisation encoded qubit in the  $|\pm\rangle$  basis.

there is one photon in each input, there are four possible output counts 0, 1, 2. If the input photons have the same polarisation (HH or VV), they are either both reflected or both transmitted. In either case we can only get a count of 1. This occurs with probability 0.5. If the photons have different polarisation we get HOM interference and can only get counts 0, 2. A count of 0 or 2 takes us out of the qubit code space for the transmitted photon and we regard these as ‘failure’. Conditioning on a single count, either

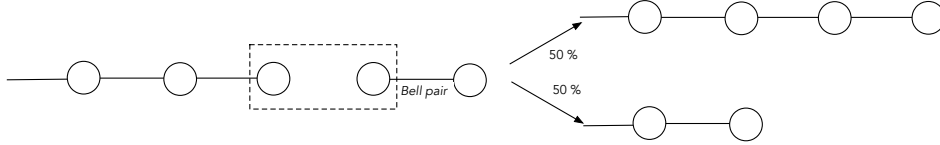


Figure 7: An illustration of joining a Bell pair to a cluster state using the non deterministic protocol of fusion gates.

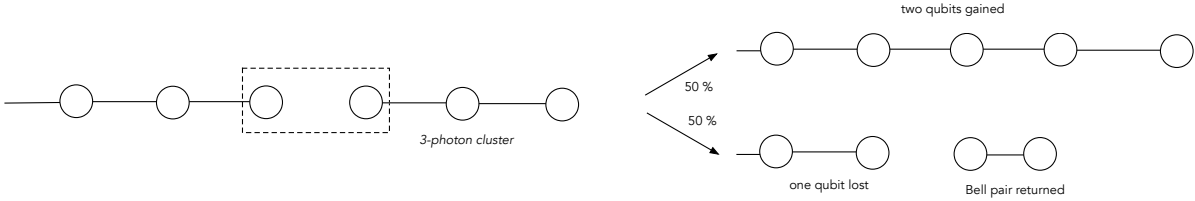


Figure 8: An illustration of how type-I fusion can be used to join two clusters together.

$H$  or  $V$ , with probability = 0.5 implements the conditional Krauss operation  $\hat{K}_{\pm} = |0\rangle\langle 00| \pm |1\rangle\langle 11|$  on the original input state. Failure of the fusion is heralded by the counts ( $n = 0, 2$ ). That is to say, if the input state was an arbitrary two qubit state  $|\psi\rangle$ , the successful conditional states are

$$|\psi\rangle_{1,out} = \hat{K}_{\pm}|\Psi\rangle_{12} \quad (29)$$

If each of the input modes encode qubits from disjoint cluster states then, when the fusion is successful, the initially separate cluster qubits become a single *fused* cluster qubit which inherits all the cluster state bonds of the two qubits which were input. Thus, if the Type-I fusion is applied to the end qubits of linear (i.e., one-dimensional) clusters of lengths  $n$  and  $m$ , success generate a linear cluster of length  $n + m - 1$ . A failure of type-I fusion effectively makes a measurement of each input qubit in the computational basis. As we noted above, this simply cuts the measured qubit from the cluster leaving all other bonds uncut. This is illustrated in Fig. 8. Given a source of SPDC polarization entangled Bell states, Type-I fusion generates arbitrarily long linear cluster states.

Clearly this procedure does not increase the size of the cluster on average. However we can use four Bell pairs, on average, to create a three qubit cluster. On average, the cluster increases by half qubit. To add one qubit to the cluster we need need  $2 \times 4 - 1 = 7$  Bell pairs, thus, 6.5 Bell pairs per added qubit.

This enables one dimensional cluster states to be formed, but we need two-dimensional cluster states for arbitrary quantum computation. Brown and Rudolph (Browne and Rudolph [2005]) came up with an ingenious scheme for doing this using a modification of the fusion gate just discussed. The scheme is illustrated in Fig. 9. Very conveniently, implementation of Type-II fusion does not require photon-number resolving detection.

When we make a Pauli  $X$  measurement on a qubit in a cluster it has an interesting effect. It does not cut the cluster, but combines the adjacent qubits into a single two-photon encoded qubit, retaining the bonds attached to each. This can be used for redundant encoding: encode a logical qubit in several qubits. The 2-qubit redundant encoding is  $|0\rangle = |0\rangle|0\rangle$  and  $|1\rangle = |1\rangle|1\rangle$ . A single qubit  $\sigma_x$  measurement in a linear cluster joins the neighbouring qubits into a single logical qubit, redundantly encoded.

Given the measurement scheme in Fig.9, when we measure both outputs it is described by the Krauss operators  $|++\rangle + |--\rangle = |00\rangle + |11\rangle$  or  $|++\rangle - |--\rangle = |00\rangle - |11\rangle$ . If one of the qubits input to Type-II fusion is redundantly encoded, we get a fusion of the other links with probability is 50%. Failure does not destroy the cluster. It cuts it or removes qubits. It simply means we need to try again. There is no back-propagation of errors through the cluster. By combining these two fusion gates, and using

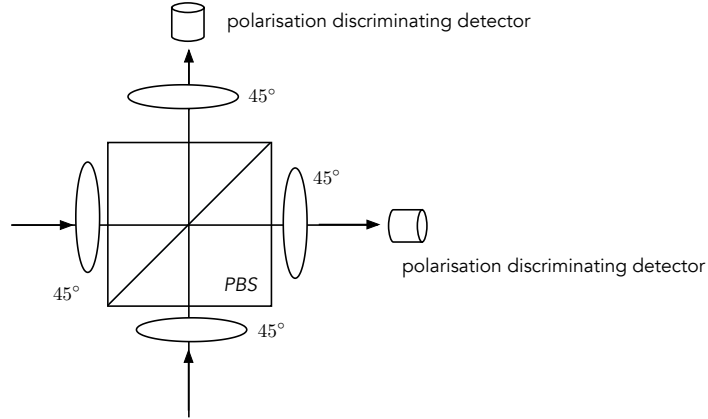


Figure 9: A type-II fusion gate measures both outputs of a polarising beamsplitter. Clearly this operation consumes two photons. If it is used when the inputs represents a qubit encoded in a two-photon state — called redundant encoding — there are four photons in and two photons out. When on and only one photon is detected at each output, we get a maximally entangled state of two photons out. This is a success. If it fails — no photon detected in either output — it corresponds to an effective Pauli  $X$  measurement.

redundantly encoded multi-photon qubits, we can generate two-dimensional qubit cluster states. This leads to a dramatic cut in the number of operations. For an arbitrary two-qubit gate, the teleportation scheme of KLM needs on average a 100-photon KLM teleportation resource state. Nielsen’s scheme needs 54 8-photon KLM teleportation resource. The Browne-Rudolph scheme needs, on average, 52 2-photon Bell states. We now need to consider in more detail the requirement for all LOQC schemes. These are

- high rate source of 2-photon Bell pairs.
- high rate source of single photon.
- number resolving single photon detectors.
- building optical circuits on a chip to enable scale-up.

A blue-print for this is presented in (Bartolucci et al. [2023]).

## 7 CV optical quantum computation

We now turn to encoding optical qubits in superposition of observables with a continuous spectrum (see Section 5.2). In the case of optical systems these are the in-phase and quadrature-phase electric field operators for an optical mode defined in Eq. (8). As for photonic qubits CV encoding is usually done using conditional (nondeterministic) gates due to the present lack of large optical nonlinearities required to do so deterministically. In CV quantum computation the key resource is a non Gaussian state.

The probability amplitude,  $\psi(q)$  determines the probability density for arbitrarily accurate measurements of the amplitude operator  $\hat{q} = (a + a^\dagger)/\sqrt{2}$  as  $P(q) = |\psi(q)|^2$ . If  $\psi(q)$  is non Gaussian, the corresponding quantum state,  $|\psi\rangle$ , is called non Gaussian. In such cases the Wigner representation of the state in phase space is also non Gaussian. The corresponding probability amplitude,  $\tilde{\psi}(p)$  for measurement of the canonically conjugate quadrature amplitude,  $\hat{p} = -i(a - a^\dagger)/\sqrt{2}$ , is given by the Fourier transform of  $\psi(q)$  (see Section 5.2). In our notation  $\hat{q}, \hat{p} = i$ . In the  $q$ -representation the action of these

operators is

$$\hat{q}|\psi\rangle \leftrightarrow q\psi(q) \quad (30)$$

$$\hat{p}|\psi\rangle \leftrightarrow -i\frac{d}{dq}\psi(q) \quad (31)$$

This implies that the  $\hat{p}$  is the generator of translations in  $\hat{q}$ , and  $\hat{q}$  is the generator of translations in  $\hat{p}$

$$e^{-iq\hat{p}}|\psi\rangle \leftrightarrow \psi(q+Q) \quad (32)$$

$$e^{-iP\hat{q}}|\psi\rangle \leftrightarrow \tilde{\psi}(p+P) \quad (33)$$

If a state is Gaussian it remains so under these translations. More generally we define the phase-space displacement operator  $D(\alpha) = \exp(\alpha a^\dagger - \alpha a)$  where  $\alpha = Q + iP$ . This also takes Gaussian states to Gaussian states. The only other unitary operator that transforms single mode Gaussian states to Gaussian states is the squeezing operator  $S(\xi) = \exp[(\xi^* a^2 - \xi a^{\dagger 2})/2]$ . In the case of two modes, we can deterministically generate entangled Gaussian states using the operators that are likewise quadratic in the two bosonic amplitude operators. An important example is the two-mode unitary  $U(\theta) = \exp[-i\theta\hat{q}_1\hat{q}_2]$ . In many ways, this is the CV equivalent of a  $ZZ$  gate. For a thorough discussion of these unitary Gaussian transformations see (Su et al. [2019]).

Braunstein and Lloyd (Lloyd and Braunstein [1999]) proved that we need to add a generator that is quartic in the amplitude operators, such as the Kerr nonlinearity  $(a^\dagger a)^2$ , to the set of linear and quadratic operators to leave the class of Gaussian states using unitary transformations. However we can also do it using nonunitary (measurement-based) transformations that describe state transformations under conditional measurement. This shifts the nonlinearity into the measurement interaction itself.

Measurement of the canonically conjugate quadrature amplitude operators  $\hat{q}, \hat{p}$  is done via homodyne detection. This requires mixing the signal with a coherent local oscillator (LO) field on a balanced beam-splitter. The LO has the same carrier frequency as the signal but is phase-shifted by  $\theta$ . If the resulting homodyne current is integrated, the result is a real random variable corresponding to a measurement of the operator  $\hat{X}(\theta) = (ae^{i\theta} + a^\dagger e^{-i\theta})/\sqrt{2}$  (Wiseman and Milburn [2009a]). Thus  $\hat{q} = \hat{X}(0), \hat{p} = -\hat{X}(\pi/2)$ .

GKP states can be prepared non deterministically via homodyne detection using a *probe* optical mode  $b, b^\dagger$  coupled to the signal mode via the interaction

$$H = \hbar\chi\alpha(a^\dagger + a)b^\dagger b \quad (34)$$

where  $a, a^\dagger$  are the annihilation and creation operators of the *signal mode* and  $b, b^\dagger$  are the annihilation operators for the *probe mode*. This is only linear in the signal mode but is quadratic in the probe mode. It is the standard interaction for opto-mechanical systems (Bowen and Milburn [2015]). The signal mode is prepared in a squeezed state

$$|\psi_{in}\rangle = S(r)|0\rangle \quad (35)$$

and the probe mode is prepared in a coherent state  $|\beta\rangle$  with  $\beta \in \mathbb{C}$ . We choose a phase convention such that  $\alpha$  is real and  $r > 0$ . This implies a phase squeezed state, that is to say, the quadrature phase amplitude in phase with the coherent displacement is anti-squeezed.

After a fixed interaction we project the probe mode into an eigenstate of  $\hat{q}_b = (b + b^\dagger)$ . This is equivalent to homodyne detection. Let the result of this measurement be  $y \in \mathbb{R}$ . The (unnormalised) conditional state of the signal mode is then given by

$$|\tilde{\psi}_{out}\rangle = \hat{\Upsilon}(y)|\psi_{in}\rangle \quad (36)$$

where the Krauss operator is given by

$$\hat{\Upsilon}(y) = {}_b\langle y|e^{-i\theta(a^\dagger+a)b^\dagger b}|\beta\rangle_b \quad (37)$$

where  $\theta = \chi\alpha T$  for interaction time  $T$ . This operator is diagonal in  $\hat{q} = a + a^\dagger$ , and has matrix elements

$$\Upsilon(q|y) = (2\pi)^{-1/4} \exp [iyr \sin(\theta q - \phi) - (y - 2r \cos(\theta q - \phi))^2/4] \quad (38)$$

This is a conditional probability amplitude, and

$$|\Upsilon(q|y)|^2 = (2\pi)^{-1/2} \exp [-(y - 2r \cos(\theta q - \phi))^2] \quad (39)$$

is a conditional probability with  $\beta = |\beta|e^{i\phi}$ .

The unnormalised conditional output state, conditioned on the measurement result  $y$ , in the diagonal representation of  $\hat{q}$  is

$$\tilde{\psi}^{(\phi)}(q|y) = \Upsilon(q|y)\psi_{in}(q) \quad (40)$$

Normalising the state we see that

$$\psi^{(\phi)}(q|y) = \frac{1}{\sqrt{\mathcal{P}(y)}} \Upsilon(q|y)\psi_{in}(q) \quad (41)$$

where

$$\mathcal{P}(y) = \int_{-\infty}^{\infty} dq |\Upsilon(q|y)|^2 |\psi_{in}(q)|^2 \quad (42)$$

is the probability distribution of the measurement outcomes. The mean and variance of this distribution are

$$\mathbb{E}(y) = 2r\langle \cos(\theta\hat{q} - \phi) \rangle \quad (43)$$

$$\mathbb{V}(y) = 1 + 4r^2(\langle \cos^2(\theta\hat{q} - \phi) \rangle - \langle \cos(\theta\hat{q} - \phi) \rangle^2) \quad (44)$$

Clearly  $\langle \cos^2(\theta\hat{q} - \phi) \rangle \leq 1$  thus  $\mathbb{V}(y) \leq 1 + 4r^2$ . There two special cases  $\phi = 0, \pi/2$  and define correspondingly  $\hat{C} = \cos(\theta\hat{q})$  and  $\hat{S} = \sin(\theta\hat{q})$ . If we take the input state as a squeezed vacuum state,  $\langle \hat{C} \rangle = e^{-\sigma\theta^2}$  and  $\langle \hat{S} \rangle = 0$  Thus in the case that  $\phi = 0$  we have that

$$\mathbb{E}(y) = 2re^{-\sigma\theta^2} \quad (45)$$

In Fig. 10 we plot the position probability density of the output state. This shows a finite energy approximation to a GKP state.

## 7.1 Gaussian boson sampling

A very important class of non Gaussian states can be generated using Gaussian boson sampling (Hamilton et al. [2017]). This relies on the ability to prepare single mode squeezed states, entangled by Gaussian unitary transformations (an LOQC network), with number-resolving photon counting for post-selection (Bourassa et al. [2021]). This approach can produce cluster states using GKP state enabling MBQC in a fault tolerant way, at least in principle.

A simple scheme for producing a small GKP state using GBS is shown in Fig. 11. The analysis of this GBS scheme is given in (Su et al. [2019]). The heralded output state is a superposition of a finite number of Fock states, followed by a squeezing operation, parametrised by  $\xi_1$  and a displacement, parametrised

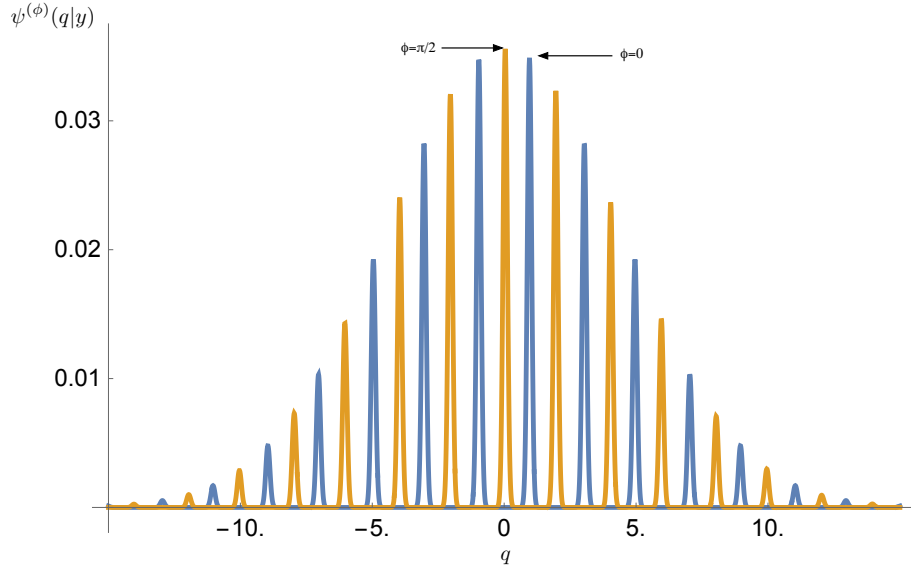


Figure 10: The probability density of the conditional output state with  $y = 0.5, \sigma = 20, \theta = \pi/2$ .

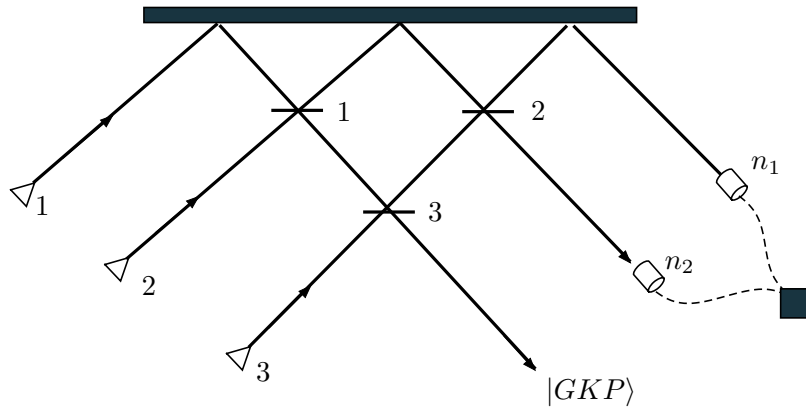


Figure 11: An optical Gaussian Boson Sampling scheme for producing an approximation to a GPK state, conditioned in the correct count string  $(n_1, n_2, n_3)$ . The inputs are single mode displaced squeezed vacuum states.

by  $d - 1$ ,

$$|\psi\rangle_{out} = D(d_1)S(\xi_1) \sum_{n=0}^{n_{max}} c_n |n\rangle. \quad (46)$$

By carefully adjusting the parameters of each of the three beamsplitters, the output state can be made a good approximation to a GKP state with a Gaussian envelope for a particular count pattern.

An early proposal using nondeterministic teleportation gates for cat state codes was given in (Ralph et al. [2003]). Many more schemes have been proposed. Parity cat states are defined as

$$|\pm\rangle = \mathcal{N}_{\pm}(|\alpha\rangle \pm |-\alpha\rangle) \quad (47)$$

where the normalisation constant is given by  $\mathcal{N}_{\pm}^{-1/2} = \sqrt{2} (1 \pm e^{-2|\alpha|^2})$ . They are eigenstates of the parity operator  $\Pi = e^{-i\pi a^\dagger a}$ . The qubit code is then simply  $|0\rangle = |+\rangle, |1\rangle = |-\rangle$ . Cat states produced nondeterministically can easily be entangled on beamsplitters (Ralph et al. [2003]), thus entangling gates are easy. Single qubit gates are more difficult but can be done using weak displacements and teleportation (Ralph et al. [2003]). Kerr nonlinearities can produce cat states with Poisson statistics (Milburn [1989b]). Such nonlinearities can be large in superconducting quantum circuits, but are too small for optical

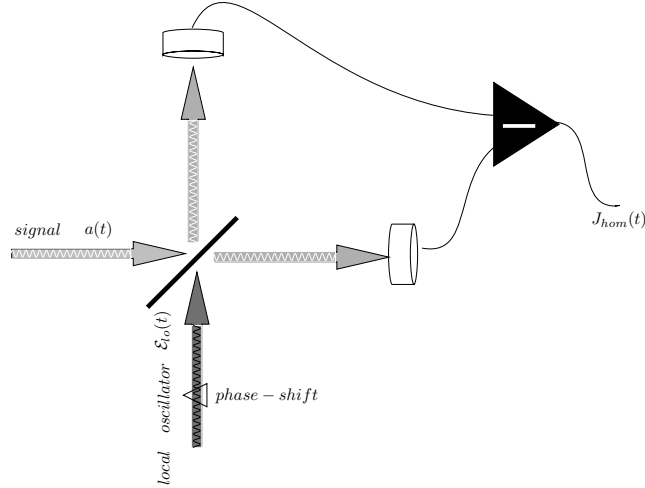


Figure 12: Balanced homodyne detection. A weak signal field with positive frequency components  $a(t)$  is combined with a strong local oscillator in a coherent state with the same carrier frequency as the signal field. Both outputs are directed to photodetectors and the resulting currents combined by subtraction in an electronic mixer. The output current is called the homodyne current.

systems. In that case nondeterministic (measurement-based) protocols can be used (Takase et al. [2021]). These only require single-mode squeezed states (a Gaussian resource) and number-resolving detection. This approach is promising for scalability (Bourassal et al. [2021]).

## 8 Detection

Detection in photonic quantum computing can be divided into homodyne detection and photon-number detection. In both cases, a photodetector converts photons to electrons, and the resulting electric current is processed to give either a quadrature measurement or a photon number.

As mentioned in Section 7, the quadrature amplitude operators  $\hat{q}$  and  $\hat{p}$  are measured via homodyne detection. The signal to be measured is spatially overlapped on a 50-50 beamsplitter with a local oscillator field (the probe mode) that is of the same frequency but phase-shifted by  $\theta$  (Fig. 12). In practice, the LO field could come from the laser that pumps the nonlinear crystal that generates the squeezed states. The LO can be phase-shifted simply by adjusting the length of one arm of the interferometer or by fine control of a glass plate in the LO arm. The expectation value of the photocurrent (normalised by the amplitude of the LO)  $J_{\text{hom}}(t)$  is

$$J_{\text{hom}}(t) = \langle e^{i\theta} a(t) + e^{-i\theta} a(t)^\dagger \rangle + \xi(t) \quad (48)$$

$$= \sqrt{2} \langle \hat{X}_\theta(t) \rangle + \xi(t) \quad (49)$$

where  $\hat{X}_\theta(t) = \hat{q}(t) \cos \theta - \hat{p}(t) \sin \theta$  and  $\xi(t)$  is white noise. The photocurrent is proportional to the expectation value of the quadrature  $\hat{q}$  (Wiseman and Milburn [2009b]). The Fourier transform of two-time (stationary) correlation function for the homodyne current enables us to define a noise power spectrum  $S(\omega)$ . We find that

$$\langle : \Delta \hat{X}_\theta^2 : \rangle = \frac{1}{2} \int_{-\infty}^{\infty} d\omega (S(\omega) - 1) \quad (50)$$

where the left hand side is the normally ordered variance in  $\hat{X}_\theta$ .

Importantly, Eq. 49 allows the measurement of either the amplitude quadrature (when  $\theta=0$ ) or

the phase quadrature (when  $\theta=\pi/2$ ). For coherent states, which have the same uncertainty in both quadratures, there is no particular advantage to using a homodyne detector. For squeezed states, which have different uncertainties in different quadratures, the homodyne detector is necessary. This technique works for both bright squeezed light or squeezed vacuum states.

The integrated homodyne current,

$$\int_0^\infty J_{hom}(t)dt \quad (51)$$

is a random variable. It can be shown that the statistics of this random variable is determined by the marginal quantum statistics of  $\hat{X}_\theta$  at  $t = 0$  (Wiseman and Milburn [2009a]).

Measurements in DV optical quantum computation require the detection of photons. This can be further divided into two. The first type distinguishes between “nothing” and “some photons”, this is also called a bucket detector. The second type can distinguish between different photon number, hence the name photon number-resolving detector. A photon detector has an efficiency  $\eta \in [0, 1]$ , defined as the probability that a photon count registers when a single photon is incident on the detector. Single photon detectors are therefore modeled as having before them a beamsplitter that has a transmission coefficient of  $\eta$ , and a reflection coefficient of  $1 - \eta$ . The incident quantum state to a photon detector is a superposition of different number states. The measurement describing a bucket detector, where 0 denotes no count, and 1 denotes a count, is given by

$$\hat{E}_0 = \sum_{n=0}^{\infty} (1 - \eta)^n |n\rangle\langle n| \quad \hat{E}_1 = \sum_{n=0}^{\infty} [1 - (1 - \eta)^n] |n\rangle\langle n|. \quad (52)$$

In general, a photon number-resolving detector makes the measurement (Scully and Willis E Lamb [1969])

$$\hat{E}_n = \sum_{k=n}^{\infty} \binom{k}{n} \eta^n (1 - \eta)^{k-n} |k\rangle\langle k|. \quad (53)$$

There is also a small probability that a count is registered even when no photons are incident, this leads to dark counts. A good photon detector has high efficiency and low dark counts. The most convenient single photon detectors are silicon avalanche photodiodes (APDs) that are operated on Geiger mode. A photon hitting the APD triggers the emission of an electron into the conductance band. The electron is accelerated in an electric potential to induce an avalanche of secondary electrons. The resulting current indicates the presence of the photon. The avalanche is stopped by reversing the electric potential leading to some dead time in the detector. Typical APDs have a dead time of a few nanoseconds and dark counts that are about  $\sim 100$  a second. Silicon APDs are convenient because they operate at room temperature, but their efficiency is limited to about  $\sim 65\%$  in the mid-infrared, and have low efficiencies for telecom wavelengths. InGaAs detectors are used for telecom wavelengths, with typical efficiencies of 10% to 30%, and dark counts typically at  $\sim 1000$ s per second.

The efficiency of single-photon detection improved greatly with the advent of superconducting nanowire single photon detectors which consist of a meandering superconducting material on a substrate, as in (see Fig. 13). Superconducting nanowire single photon detectors (SNSPDs) have efficiencies of  $\sim 90 + \%$  (Marsili et al. [2013]). SNSPDs operate near the critical current ( $I_B$ ) to be at the superconducting phase. The absorption of a photon causes the device to have a higher resistivity, leading to a voltage spike that is considered as the photon detection (see Fig. 13.c). The dead time of an SNSPD is similar to that of an APD, and the timing jitter is very small (in the few ps range). The increase in efficiency comes at the price of a more complicated setup that involves a cryostat, because the operating temperatures to reach superconductivity are between 0.8 to 3 K. The specific wavelength range that the SNSPD is sensitive to is determined by the choice of the superconducting material and the optical cavity around

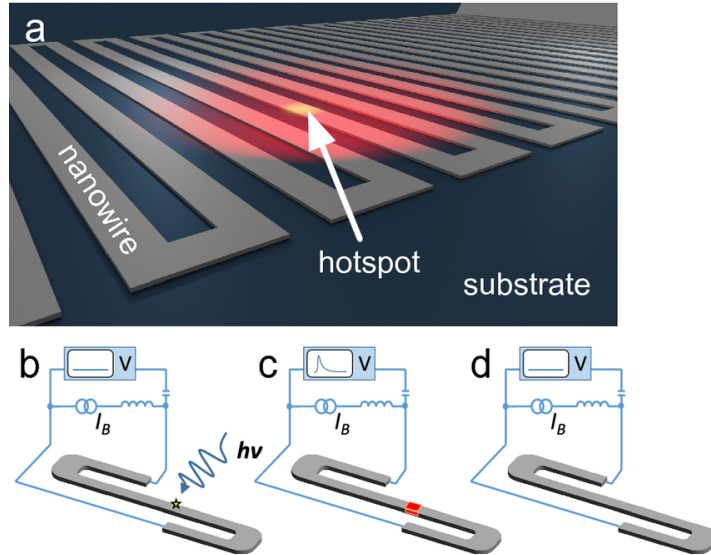


Figure 13: SNSPD working principle. The SNSPD is operated near the critical temperature. Absorption of a photon causes a hotspot to develop (a). The nanowire is normally superconducting and DC bias  $I_B$  is applied (b). The hotspot induces additional current and the critical current density is surpassed, a voltage peak is registered (c). The heat is then dissipated, and the SNSPD is ready for detection again (d). (Figure lifted from (Fuchs et al. [2022]), used under CC by 4.0.)

it. SNSPDs are bucket detectors, photon-number resolution using is limited by the saturation of the avalanche process. However, it has been shown recently that analysing the timing of the rising and falling edges of the output pulses give some degree of photon-number-resolution, although only for low photon numbers ( $\sim 4$ )(Sauer et al. [2023]).

Photon-number resolution is possible using another kind of superconducting detector—transition-edge sensors (TESs). Photon-number-resolution is possible in a TES because the change in resistivity is proportional to the number of photons absorbed. The TES acts as a very sensitive bolometer. The number of photons can be read out by integrating the current produced as a result of the change in resistivity. Recent results have show photon-number-resolution of up to  $\sim 20$  (Harder et al. [2016]). The efficiency of TESs is comparable to that of SNSPDs. The dark count rates are lower, but the dead time (in the  $\mu\text{s}$  range) and timing jitter (in the ns range) are greater than that of an SNSPD (Lamas-Linares et al. [2013]). As seen in Section 7.1, photon-number-resolution is needed in the preparation of the GKP states, hence the great interest in developing this type of detectors.

One subtlety that deserves mentioning is that the detection for CV optical quantum computing assumes that the input and output modes are perfectly mode-matched—the detector is sensitive to all the input modes. This is different from the case of DV where some mode filtering (e.g. a polarising beamsplitter or a multiplexer) that depends on the encoding used is often placed before the photodetector.

## 9 Large-scale photonic quantum computing

### 9.1 Single photon sources

Scalable optical quantum computing require single photon sources. A single-photon state is a coherent superposition of a single excitation over many frequency modes(Raymer and Walmsley [2020]). We will restrict the discussion to multi-mode fields with plane polarisation. The positive frequency components

of the field are,

$$E^{(+)}(t, \vec{x}) = \int_0^\infty d\omega \tilde{a}(\omega) e^{-i(\omega t - \vec{k} \cdot \vec{x})} \quad , \quad (54)$$

where  $\tilde{a}(\omega), \tilde{a}^\dagger(\omega')$  are bosonic annihilation/creation operators satisfying

$$[\tilde{a}(\omega), \tilde{a}^\dagger(\omega')] = \delta(\omega - \omega'), \quad (55)$$

and  $\omega = c|\vec{k}|$ .

We will assume that all modes are in the vacuum except for those propagating in the  $+x$  direction with a carrier frequency centred on  $\omega = \Omega$  and a frequency bandwidth  $B$  much less than the carrier frequency. In that case we can change the frequency variable to  $\omega \rightarrow \omega - \Omega$  and extend the lower limit of integration over the displaced variable to  $-\Omega \rightarrow -\infty$ . We will refer to this set of approximations collectively as the ‘quantum optics approximation’. We then only need consider those modes that contribute to the positive frequency operate defined as

$$a(t - x/c) = \int_{-\infty}^\infty d\omega \tilde{a}(\omega) e^{-i\omega(t-x/c)} \quad . \quad (56)$$

In this form the operators  $a(t)$  and  $\tilde{a}(\omega)$  appear as Fourier transform pairs. In our units  $a(t)$  has units of  $s^{-1/2}$  which ensures that  $\langle a^\dagger(t)a(t) \rangle$  has units of a rate. In what follows we will assume the detector is located at  $x = 0$ .

We define an single-photon (pure) state as a superposition of a single excitation over many frequencies,

$$|\xi\rangle = \left[ \int_{-\infty}^\infty d\omega \tilde{\xi}(\omega) \tilde{a}^\dagger(\omega) \right] |0\rangle \quad . \quad (57)$$

Here  $\tilde{\xi}(\omega)$  is the probability amplitude that there is a single photon in a frequency band between  $\omega$  and  $\omega + d\omega$ . Normalisation of the state requires that

$$\int_{-\infty}^\infty d\omega |\tilde{\xi}(\omega)|^2 = 1 \quad (58)$$

The average field amplitude of a single photon state is zero,

$$\langle 1|a(t)|1\rangle = 0 \quad . \quad (59)$$

However the intensity is not zero,

$$n(t) = \langle a^\dagger(t)a(t) \rangle = |\xi(t)|^2 \quad , \quad (60)$$

where

$$\xi(t) = \int_{-\infty}^\infty d\omega e^{-i\omega t} \tilde{\xi}(\omega) \quad . \quad (61)$$

The fact that  $n(t)$  appears as the modulus square of a single, complex valued function in Eq. (60) is a reflection of the underlying purity of the single photon state. In optical terms we would say that the pulse is ‘transform limited’ although we need to bear in mind that this is highly non classical state with an average field amplitude of zero. The key signature of a true pure-state single photon source is provided by Hong-Ou-Mandel (HOM) interference (Hong et al. [1987]).

HOM interference is a fourth order interference effect. If two identical single photons arrive on a 50/50 beam-splitter the probability to detect a single photon at each of the two output ports - a coincidence

- is zero. This is because there are two indistinguishable ways this event can occur: both photons are reflected or both photons are transmitted and the probability amplitudes for each of these paths cancel exactly in the ideal case. If we introduce a time delay between the two photon pulses, the probability to detect a coincidence drops from a value of 0.5 to near zero as the time delay is reduced to zero.

In Figure 14, we show a HOM scheme with two input fields with positive frequency components  $a_{in}(t), b_{in}(t)$  and two output fields determined by

$$a_{out}(t) = \frac{1}{\sqrt{2}}(a_{in}(t) + b_{in}(t)) \quad (62)$$

$$b_{out}(t) = \frac{1}{\sqrt{2}}(a_{in}(t) - b_{in}(t)) \quad (63)$$

The change in sign of the second equation here is an indication of the time reversal invariance of an ideal

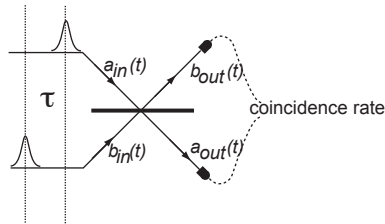


Figure 14: A scheme for a Hong-Ou-Mandel interference experiment. A beamsplitter couples two input field modes to two output field modes. The input field modes are prepared in identical single photon pulses and a variable time delay  $\tau$  is introduced. Detectors placed in the path of the output field modes show a suppression of coincidence events when the delay time is zero.

beamsplitter. Assume that at  $t = 0$  the a-mode is prepared in the single photon state with amplitude function  $\xi_a(t)$  while the b-mode is prepared in a single photon state at  $t = \tau$  with amplitude function  $\xi_b(t - \tau)$ . To be specific we will choose,

$$\xi(t) = \begin{cases} \sqrt{\gamma}e^{-\gamma t/2} & t \geq 0 \\ 0 & t < 0 \end{cases} \quad (64)$$

The joint probability to count one photon in output mode-a and one photon in output mode-b is defined by

$$P_{ab} = \int_0^\infty \int_0^\infty \langle a_{out}^\dagger(t) b_{out}^\dagger(t') b_{out}(t') a_{out}(t) \rangle dt dt' \quad (65)$$

In this case we find that this is a function of  $\tau$  and is given by

$$P_{ab}(\tau) = \frac{1}{2} \left( 1 - e^{-\gamma|\tau|} \right) \quad (66)$$

A good example of a single photon source which exhibits both a suppression of second order correlation at zero time and good HOM interference visibility was demonstrated by the group of Rempe(Keller et al. [2004]) in Garching and also by the group of Kuhn at Oxford (Nisbet-Jones et al. [2013]). The experiments of Rempe(Keller et al. [2004]) and Kuhn(Nisbet-Jones et al. [2013]) verified the temporal shape of their photon amplitudes and phases in detection-time resolved HOM and quantum homodyne experiments.

For scalable optical quantum computing single photon sources need to be integrated into a device. Single photons sources for measurement based protocols, such as fusion, are being developed across a number of technologies, such as doped fibres(Shimizu et al. [2024]), diamonds(Flatae et al. [2024]), and semiconductor-based sources(Senellart [2021]). The performance benchmarks require very good control over rate of emission and control of the spatio-temporal mode functions of each photon. These translate

into an efficiency metric for achieving near quantum purity over many trials. There are already many commercial single-photon source developers and new technologies for quantum optical sources are likely to emerge in coming years.

## 9.2 Error correction

For all quantum computing technologies the challenge is to implement error correction to enable large scale fault tolerant computation(Brun [2020]). The discovery of quantum error correction by Calderbank and Shor(Calderbank and Shor [1996]) and independently by Steane(Andrew [1996]) was the main reason why quantum computing has not remained little more than a curious quantum phenomenon and instead has moved to the technological frontier attracting billions of dollars in funding. The largest technological challenge for optical QC schemes is photon loss. The solution is to understand photon loss as a qubit error and find error correction codes to reduce the probability for that error(Brun [2020]).

Much is known about the kinds of code that will be useful in quantum optical schemes. The fusion gate approach suggests a number of new ways to implement surface codes in measurement based quantum computation. The error correction methods developed by PsiQuantum can tolerate a 2.7% probability of suffering a single photon loss(Bartolucci et al. [2023]). These methods, implemented in integrated photonic devices, offer a clear path to very large scale QC. Measurement based quantum computing for continuous variables under development at Xanadu also suggest specific quantum error correction protocols. Scale-up of GBS machines is proceeding rapidly(Madsen et al. [2022]). These offer significant non-classical capability without error correction(Walmsley [2023]).

## 10 Quantum machine learning

There is a developing awareness that the current paradigm for quantum computation based only on qubit circuits may not be the best approach to harnessing the quantum world for computational tasks, especially machine learning(Fernandez [2024]). The current quantum computing paradigm closely follows the classical computational model based on CMOS digital logic circuits and von Neumann architecture. The rise of machine learning provides another impetus to reconsider the current computational paradigm. The cost of machine learning is largely associated with the energy cost of implementing a von Neumann architecture on CMOS digital computers(Chojnacka [2021]).

In recent years the idea of using physical systems,, especially quantum systems, to perform computational task has resurfaced(Kaiser and Datta [2021]; Coles et al. [2023]; Wang et al. [2022]). Of particular interest is the approach of *Normal Computing* and *Extropic*(Coles et al. [2023]; ext [2024]). They give a framework for physics-inspired AI algorithms based on probabilistic switching in physical devices. Machine learning algorithms can be viewed as a data analysis and statistical tools for finding patterns in data. There are quantum optical versions of deep neural networks(Steinbrecher et al. [2019]; Zhu et al. [2024]; Ma et al. [2023]), convolutional neural networks(Zapletal et al. [2023]) and kernel embedding(Bowie et al. [2023]).

A very early physical machine approach was developed by DWave in the early 2000s. It is best described as an annealing computational machine using dissipative quantum tunnelling between localised states(King et al. [2022]). It is based on finding steady states that are close to many-body ground states that happen to solve an optimization problem. However there is no reason to restrict quantum steady states to such states. Far-from-thermal-equilibrium steady states offer greater possibilities and quantum phase transitions at low temperature can be easily exploited in quantum optics. An example of this is the coherent Ising machine approach developed by Yamamoto and coworkers(Yamamoto et al. [2017]), but has yet to reach a clear quantum advantage.

An exciting recent development is the rise of hardware implementations of machine learning using optical systems. These will move rapidly to quantum optical demonstrations. Raman quantum memories, in atomic (Heshami et al. [2016]) or optomechanical systems (Lake et al. [2021]), offer a possible path to quantum convolutional neural networks, if they can be made to work at the single photon level. The technological dividend of single photon computing could deliver a huge increase in the thermodynamic efficiency of AI (Ma et al. [2023]; Wang et al. [2022]). There is no need for cooling. The world is already very cold at optical frequencies.

## Conclusion and Outlook

Optical quantum computing is clearly on a path to controlling hundreds of error protected logical qubits. No matter what technology platform eventually wins in the market for commercial quantum computing, optical technology will always be required for quantum interconnects. It will be advantageous to do some computational processing in the optical in-line networks. In the early 1980s much was made of the possibility of using classical optics for computation. It did not go away; it became incorporated into the optical fibre communication system. Optical quantum computation may be similar (McMahon [2023]).

## References

- (2024). Extropic. <https://www.extropic.ai/future>.
- Andrew, S. (1996). Multiple-particle interference and quantum error correction. *Proceedings of the Royal Society of London A*, 452:2551.
- Bartolucci, S., Patrick, B., Bombín, H., Cable, H., Dawson, C., Gimeno-Segovia, M., Johnston, E., Kieling, K., Nickerson, N., Pant, M., Pastawski, F., Rudolph, T., and Sparrow, C. (2023). Fusion-based quantum computation. *Nature Communications*, 14:912.
- Bourassa, J. E., Alexander, R. N., Vasmer, M., Patil, A., Tzitrin, I., Matsuura, T., Su, D., Baragiola, B. Q., Guha, S., Dauphinais, G., Sabapathy, K. K., Menicucci, N. C., and Dhand, I. (2021). Blueprint for a scalable photonic fault-tolerant quantum computer. *Quantum*, 5:392.
- Bourassal, E., Alexander, R., Vasmer, M., Patil, A., Tzitrin, I., Matsuura, T., Su, D., Baragiola, B., Guha, S., Dauphinais, G., Sabapathy, K., Menicucci, N., and Dhand, I. (2021). Blueprint for a scalable photonic fault-tolerant quantum computer. *Quantum*, 5:392.
- Bowen, W. and Milburn, G. (2015). *Quantum Optomechanics*. CRC Press.
- Bowie, C., Shrapnel, S., and Kewming, M. J. (2023). Quantum kernel evaluation via hong–ou–mandel interference. *Quantum Science and Technology*, 9(1):015001.
- Briegel, H., Browne, D., Dür, W., Raussendorf, R., and Van Den Nest, M. (2009). Measurement-based quantum computation. *Nature Physics*, 5:19–26.
- Browne, D. E. and Rudolph, T. (2005). Resource-efficient linear optical quantum computation. *Physical Review Letters*, 95:010501.
- Brun, T. A. (2020). Quantum error correction. In *Oxford Research Encyclopedia of Physics*.
- Calderbank, A. R. and Shor, P. W. (1996). Good quantum error-correcting codes exist. *Physical Review A*, 54:1098–1105.

- Chojnacka, R. (2021). Compute cost and environmental impact of deep learning. *Towards Data Science*.
- Coles, P. J., Szczepanski, C., Melanson, D., Donatella, K., Martinez, A. J., and Sbahi, F. (2023). Thermodynamic AI and the fluctuation frontier. *arXiv:2302.06584*.
- Devitt, S. J., Munro, W. J., and Nemoto, K. (2013). Quantum error correction for beginners. *Reports on Progress in Physics*, 76(7):076001.
- DiVincenzo, D. P. (2000). The physical implementation of quantum computation. *Fortschritte der Physik: Progress of Physics*, 48(9-11):771–783.
- Fernandez, A. M. (2024). Digital-analog quantum computing and algorithms. *arXiv:2401.10622v1*.
- Flatae, A. M., Sledz, F., Kambalathmana, H., Lagomarsino, S., Wang, H., Gelli, N., Sciortino, S., Woerner, E., Wild, C., Butz, B., and Agio, M. (2024). Single-photon emission from silicon-vacancy color centers in polycrystalline diamond membranes. *Applied Physics Letters*, 124(9):094001.
- Fuchs, S., Abel, J. J., Nathanael, J., Reinhard, J., Wiesner, F., Wünsche, M., Skruszewicz, S., Rödel, C., Born, D., Schmidt, H., et al. (2022). Photon counting of extreme ultraviolet high harmonics using a superconducting nanowire single-photon detector. *Applied Physics B*, 128(2):26.
- Gottesman, D., Kitaev, A., and Preskill, J. (2001). Encoding a qubit in an oscillator. *Physical Review A*, 64:012310.
- Hamilton, C. S., Kruse, R., Sansoni, L., Barkhofen, S., Silberhorn, C., and Jex, I. (2017). Gaussian boson sampling. *Physical Review Letters*, 119:170501.
- Harder, G., Bartley, T. J., Lita, A. E., Nam, S. W., Gerrits, T., and Silberhorn, C. (2016). Single-mode parametric-down-conversion states with 50 photons as a source for mesoscopic quantum optics. *Physical Review Letters*, 116(14):143601.
- Heshami, K., England, D., Humphreys, P., Bustard, P., Acosta, V., Nunn, J., and Sussman, B. (2016). Quantum memories: emerging applications and recent advances. *Journal of Modern Optics*, 12:2005.
- Hong, C. K., Ou, Z. Y., and Mandel, L. (1987). Measurement of subpicosecond time intervals between two photons by interference. *Physical Review Letters*, 59:2044–2046.
- Hutchinson, G. D. and Milburn, G. J. (2004). Nonlinear quantum optical computing via measurement. *Journal of Modern Optics*, 51(8):1211–1222.
- Kaiser, J. and Datta, S. (2021). Probabilistic computing with p-bits. *Applied Physics Letters*, 119(15):150503.
- Keller, M., Lange, B., Hayasaka, K., Lange, W., and Walther, H. (2004). Continuous generation of single photons with controlled waveform in an ion-trap cavity system. *Nature*, 431:1075.
- King, A. D., Suzuki, S., Raymond, J., Zucca, A., Lanting, T., Altomare, F., Berkley, A. J., Ejtemaee, S., Hoskinson, E., Huang, S., Ladizinsky, E., MacDonald, A., Marsden, G., Oh, T., Poulaine-Lamarre, G., Reis, M., Rich, C., Sato, Y., Whittaker, J. D., Yao, J., Harris, R., Lidar, D. A., Nishimori, H., and Amin, M. H. (2022). Coherent quantum annealing in a programmable 2,000 qubit ising chain. *Nature Physics*, 18:1324.
- Knill, E., Laflamme, R., and Milburn, G. J. (2001). A scheme for efficient quantum computation with linear optics. *Nature*, 409:46.

- Konno, Shunya, e. a. (2023). Propagating Gottesman-Kitaev-Preskill states encoded in an optical oscillator. *arXiv:2309.02306*.
- Lake, D. P., Mitchell, M., Sukachev, D. D., and Barclay, B. E. (2021). Processing light with an optically tunable mechanical memory. *Natural Communications*, 12:663.
- Lamas-Linares, A., Calkins, B., Tomlin, N. A., Gerrits, T., Lita, A. E., Beyer, J., Mirin, R. P., and Woo Nam, S. (2013). Nanosecond-scale timing jitter for single photon detection in transition edge sensors. *Applied Physics Letters*, 102(23).
- Lloyd, S. and Braunstein, S. L. (1999). Quantum computation over continuous variables. *Physical Review Letters*, 82:1784–1787.
- Ma, S.-Y., Wang, T., Laydevant, J., Wright, L. G., and McMahon, P. L. (2023). Quantum-noise-limited optical neural networks operating at a few quanta per activation. *arXiv:2307.15712*.
- Madsen, L., Laudenbach, F., Askarani, M. F., Rortais, F., Vincent, T., Bulmer, J. F. F., Miatto, F., Neuhaus, L., Helt, L. G., Collins, M. J., Lita, A., Gerrits, T., Nam, S. W., Vaidya, V. D., Menotti, M., Dhand, I., Vernon, Z., Quesada, N., and Lavoie, J. (2022). Quantum computational advantage with a programmable photonic processor. *Nature*, 606:75.
- Marsili, F., Verma, V. B., Stern, J. A., Harrington, S., Lita, A. E., Gerrits, T., Vayshenker, I., Baek, B., Shaw, M. D., Mirin, R. P., et al. (2013). Detecting single infrared photons with 93% system efficiency. *Nature Photonics*, 7(3):210–214.
- McMahon, P. (2023). The physics of optical computing. *Nature Reviews Physics*, page 717.
- Milburn, G. J. (1989a). A quantum optical Fredkin gate. *Physical Review Letters*, page 2124.
- Milburn, G. J. (1989b). Quantum optical Fredkin gate. *Physical Review Letters*, 62:2124–2127.
- Miller, D. A. (2019). Waves, modes, communications, and optics: a tutorial. *Advances in Optics and Photonics*, 11(3):679–825.
- Nielsen, M. A. (2004). Optical quantum computation using cluster states. *Physical Review Letters*, 93:040503.
- Nisbet-Jones, P. B., Dille, J., Ljunggren, D., and Kuhn, A. (2013). *New Journal of Physics*, 15:053007.
- Ourjoumtsev, A., Tualle-Brouni, R., Laurat, J., and Grangier, P. (2006). Generating optical Schrödinger kittens for quantum information processing. *Science*, 312(5770):83–86.
- Pittman, T. B., Jacobs, B. C., and Franson, J. D. (2002). Demonstration of nondeterministic quantum logic operations using linear optical elements. *Physical Review Letters*, 88:257902.
- Ralph, T. C., Gilchrist, A., Milburn, G. J., Munro, W. J., and Glancy, S. (2003). Quantum computation with optical coherent states. *Physical Review A*, 68:042319.
- Raymer, M. G. and Walmsley, I. A. (2020). Temporal modes in quantum optics: then and now. *Physica Scripta*, 95:064002.
- Sauer, G., Kolarczik, M., Gomez, R., Conrad, J., and Steinlechner, F. (2023). Resolving photon numbers using ultra-high-resolution timing of a single low-jitter superconducting nanowire detector. *arXiv preprint arXiv:2310.12472*.

- Scully, M. O. and Willis E Lamb, J. (1969). Quantum theory of an optical maser. iii. theory of photoelectron counting statistics. *Physical Review*, 179(2):368.
- Senellart, P. (2021). Semiconductor single-photon sources: progress and applications. *Photoniques*, 107.
- Shimizu, K., Inoue, K., Katsumata, K., Naruki, A., Sadgrove, M., and Sanaka, K. (2024). Single-photon generation from a neodymium ion in optical fiber at room temperature. *Applied Physics Letters*, 124(8):081106.
- Steinbrecher, G. R., Olson, J. P., Englund, D., and Carolan, J. (2019). Quantum optical neural networks. *npj Quantum Information*, 5:60.
- Su, D., Myers, C. R., and Sabapathy, K. K. (2019). Conversion of gaussian states to non-gaussian states using photon-number-resolving detectors. *Physical Review A*, 100:052301.
- Takase, K., Yoshikawa, J.-i., Asavanant, W., Endo, M., and Furusawa, A. (2021). Generation of optical schrödinger cat states by generalized photon subtraction. *Physical Review A*, 103:013710.
- Walls, D. F. and Milburn, G. J. (2008). *Quantum Optics*. Springer.
- Walmsley, I. (2023). Light in quantum computing and simulation: perspective. *Optica Quantum*, 1(1):35–40.
- Wang, T., Ma, S.-Y., Wright, L. G., Onodera, T., Richard, B. C., and McMahon, P. L. (2022). An optical neural network using less than 1 photon per multiplication. *Nature Communications*, 13(1).
- Wiseman, H. M. and Milburn, G. J. (2009a). *Quantum Measurement and Control*. Cambridge University Press.
- Wiseman, H. M. and Milburn, G. J. (2009b). *Quantum measurement and control*. Cambridge University Press.
- Yamamoto, Y., Aihara, K., Leleu, T., Kawarabayashi, K., Kako, S., Fejer, M., Inoue, K., and Takesue, H. (2017). Coherent ising machines—optical neural networks operating at the quantum limit. *npj Quantum Information*, 3:49.
- Yamamoto, Y., Kitagawa, M., and Igeta., K. (1988). In *In Proc. 3rd Asia-Pacific Phys. Conf., Singapore.*
- Zapletal, P., McMahon, N. A., and Hartmann, M. J. (2023). Error-tolerant quantum convolutional neural networks for symmetry-protected topological phases. *arXiv:2307.03711*.
- Zhu, H., Lin, H., Wu, S., Luo, W., Zhang, H., Zhan, Y., Wang, X., Liu, A., and Kwek, L. C. (2024). Quantum computing and machine learning on an integrated photonics platform. *Information*, 15(2).